Vol 17 No 3, March 2008
1674-1056/2008/17(03)/0927-12

Chinese Physics B

© 2008 Chin. Phys. Soc.
and IOP Publishing Ltd

The interaction between multiple bubbles and the free surface*

Zhang A-Man(张阿漫)† and Yao Xiong-Liang(姚熊亮)

School of Shipbuilding Engineering, Harbin Engineering University, Harbin 150001, *China*

(Received 15 September 2007; revised manuscript received 21 October 2007)

The flow is assumed to be potential, and a boundary integral method is used to solve the Laplace equation for the velocity potential to investigate the shape and the position of the bubble. A 3D code to study the bubble dynamics is developed, and the calculation results agree well with the experimental data. Numerical analyses are carried out for the interaction between multiple bubbles near the free surface including in-phase and out-of-phase bubbles. The calculation result shows that the bubble period increases with the decrease of the distance between bubble centres because of the depression effect between multiple bubbles. The depression has no relationship with the free surface and it is more apparent for out-of-phase bubbles. There are great differences in dynamic behaviour between the in-phase bubbles and the out-of-phase bubbles due to the depression effect. Furthermore, the interaction among eight bubbles is simulated with a three-dimensional model, and the evolving process and the relevant physical phenomena are presented. These phenomena can give a reference to the future work on the power of bubbles induced by multiple charges exploding simultaneously or continuously.

Keywords: multiple bubbles, boundary integral, free surface, depression effect, potential flow theory
PACC: 4000, 4710, 5000, 5280Q

1. Introduction

The boundary element method (BEM)[1−6] has been widely used to simulate the bubble dynamics, including the large bubbles resulting from explosion and the small cavitation bubbles. The BEM can reduce the number of dimensions to one, and only the boundary of the fluid domain needs to be meshed, which saves a lot of computing time. Moreover, the BEM can be well adapted to the large deformation of meshes at the boundaries of the structure and the bubble, even when the bubble surface generates sever distortion. In general, the BEM has its outstanding advantage in modelling the 3D complex boundary surface (e.g. the bubble surface and the free surface), therefore, it is used in this paper. In the past decades, a vast literature dealing with the bubble dynamics has been published.[1−10] But there was only a little involved with the interaction of double bubbles or multiple bubbles.[11] There exists the interaction between two bubbles in both the small bubbles and the macro large bubbles, for example, when two charges explode simultaneously. In the field of multiple charges exploding, a common knowledge is that two charges exploding simultaneously or continuously would yield higher power than a single charge. But it has not been validated. Therefore, the interaction of multiple bubbles including the in-phase bubbles and out-of-phase bubbles is simulated with a 3D code developed in this paper in order to give a reference to the relevant research on the dynamics of multiple bubbles.

2. Theoretical background

Gas inside a bubble is assumed to be isentropic, and the effect of the gas motion on its pressure is ignored. Gas pressure is related only to its initial state and volume. The relation between the bubble pressure P and the bubble volume V is as follows:

$$p = p_{\rm c} + p_0 \left(\frac{V_0}{V} \right)^{\lambda}, \tag{1}$$

where $P_{\rm c}$ is the saturated vapour pressure of condensable gas, P_0 and V_0 are the initial pressure and the initial volume of the underwater explosion bubble respectively, and γ is the ratio of the specific heat which is related to the gas composition. For gaseous explosion products from Trinotrotucl (TNT),[10] it equals

*Project supported by the National Natural Science Foundation of China (Grant No 50779007).
†E-mail: amanzhang@gmail.com

1.25; for ideal gas, it equals 1.4.

The ambient water moves along with the bubble under the effects of expansion and deformation of the bubble. Without taking the viscosity and the compressibility into account, the water can be considered as an irrotational incompressible ideal fluid. The velocity potential of the fluid domain satisfies the Laplace equation

$$\nabla^2\phi = 0. \tag{2}$$

The velocity $\boldsymbol{u}$ of the node in the fluid domain can be expressed as

$$\boldsymbol{u} = \nabla\phi. \tag{3}$$

With the boundary condition in an infinite distance, the velocity potential $\phi(\boldsymbol{p})$ at the bubble boundary satisfies the boundary integral equation

$$c(\boldsymbol{p})\phi(\boldsymbol{q}) = \iint_S \left(\frac{\partial\phi(\boldsymbol{q})}{\partial n}G(\boldsymbol{p},\boldsymbol{q}) - \phi(\boldsymbol{q})\frac{\partial}{\partial n}G(\boldsymbol{p},\boldsymbol{q})\right)\mathrm{d}S, \tag{4}$$

where S is the boundary surface including the bubble surface; $\boldsymbol{p}$ and $\boldsymbol{q}$ represent the fixed point and the integration point of the boundary, respectively; $c(\boldsymbol{p})$ is the solid angle observed at $\boldsymbol{p}$. When $\boldsymbol{p}$ is in the fluid domain, $c(\boldsymbol{p}) = 4\pi$; when $\boldsymbol{p}$ is at the smooth boundary, $c(\boldsymbol{p}) = 2\pi$; when $\boldsymbol{p}$ is in the corner, $c(\boldsymbol{p}) < 4\pi$. The solid angle at the control point $\boldsymbol{p}$ can be obtained by integration as

$$c(\boldsymbol{p}) = \iint_S \frac{\partial G}{\partial n}(\boldsymbol{p},\boldsymbol{q})\,\mathrm{d}S_q, \quad \boldsymbol{p}\in S. \tag{5}$$

The spacial Green's function is $G(\boldsymbol{p},\boldsymbol{q}) = |\boldsymbol{p}-\boldsymbol{q}|^{-1}$, and the boundary condition in an infinite distance is $|\nabla\phi\to 0|$. The coordinate is defined as shown in Fig.1. The origin is at the midpoint of the connecting line between two bubble centres. The x axis directs left and the z axis directs up.

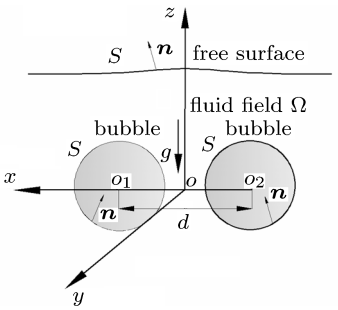


Fig.1. The coordinate system.

When the bubble surface satisfies the dynamic condition under which the pressures inside and outside the bubble are equal, the motion of the boundary can be determined as follows:

$$\frac{\mathrm{d}\boldsymbol{x}}{\mathrm{d}t} = \nabla\phi, \tag{6}$$

$$\frac{\mathrm{d}\phi}{\mathrm{d}t} = \frac{1}{2}|\nabla\phi|^2 - g(z-d), \quad \text{on the free surface,} \tag{7}$$

$$\frac{\mathrm{d}\phi}{\mathrm{d}t} = \frac{p_\infty}{\rho} + \frac{1}{2}|\nabla\phi|^2 - gz - \frac{1}{\rho}\left(p_\mathrm{c} + p_0\left(\frac{V_0}{V}\right)^\gamma\right), \quad \text{on the bubble surface,} \tag{8}$$

where g is the gravity acceleration, the original position of bubble centre is $z = d$, and p_∞ is the ambient pressure in an infinite distance horizontally. We consider R_m as the characteristic length, $\Delta p = p_\infty - p_\mathrm{c}$ as characteristic pressure to make the boundary condition dimensionless, such that

$$\frac{\mathrm{d}\phi}{\mathrm{d}t} = \frac{1}{2}|\nabla\phi|^2 - \delta^2(z-\gamma_f), \quad \text{on free surface,} \tag{9}$$

$$\frac{\mathrm{d}\phi}{\mathrm{d}t} = 1 + \frac{1}{2}|\nabla\phi|^2 - \delta^2 z - \varepsilon\left(\frac{V_0}{V}\right)^\gamma, \quad \text{on bubble surface,} \tag{10}$$

where $\delta = \sqrt{\rho g R_\mathrm{m}/\Delta p}$ is the buoyancy parameter, $\varepsilon = p_0/\Delta p$ is the initial pressure parameter of the bubble (strength parameter), and $\gamma_f = d/R_\mathrm{m}$ is the non-dimensional depth of the bubble centre. In order to generalize our research, we use $R_\mathrm{m}(\rho/\Delta P)^{1/2}$ as characteristic time, $R_\mathrm{m}(\rho/\Delta P)^{1/2}$ as characteristic velocity respectively, and $(\rho g R_\mathrm{m}/\Delta p)^{1/2}$ as characteristic buoyancy to make all variables dimensionless. For the underwater explosion bubble, parameter ε and dimensional R_m can be obtained from the existing imperial formula.[11−14] The numerical method of solving Eq.(4) has been introduced in Ref.[15].

3. Velocities and normal vectors of nodes

The velocities of the nodes at the boundary are uncertain. Normal velocities can be obtained by solving Eq.(4) but the nodal normal vectors are unknown (nodal normal does not match that of element). Node i is assumed to be a common node among several nodes, as shown in Fig.2, and then its normal vector can be obtained by averaging the normal vectors of its surrounding elements (arithmetic mean is the simplest method and the normal vector of node i is obtained by the weighting method in this paper, see

the following text). To obtain the nodal actual velocity, we use the method in Ref.[16] to establish a set of equations about the normal vector and velocity vector of node i.

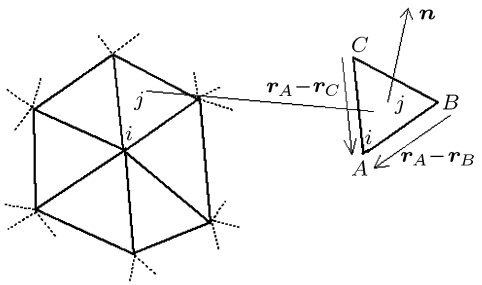


Fig.2. The node i, surrounded by 6 elements, the element j is highlighted in grey.

Considering node i composed of several elements as shown in Fig.2, we assume that the element j consists of three corners A, B and C. Node i coincides with corner A. Since element j is a plane element, normal vectors to element j are uniform. Based on these assumptions, a set of equations to evaluate the velocity $\boldsymbol{\nu}_i$ of the node i can be established as follows:

$$\begin{aligned}
&(\boldsymbol{r}_A - \boldsymbol{r}_B)\cdot\nabla\phi_j \approx \phi_A - \phi_B,\\
&(\boldsymbol{r}_A - \boldsymbol{r}_C)\cdot\nabla\phi_j \approx \phi_A - \phi_C,\\
&\boldsymbol{n}\cdot\nabla\phi_j = \frac{\partial\phi}{\partial n},
\end{aligned} \tag{11}$$

which may be rewritten in the matrix form:

$$\begin{aligned}
&\begin{bmatrix} x_A - x_B & y_A - y_B & z_A - z_B\\ x_A - x_C & y_A - y_C & z_A - z_C\\ n_x & n_y & n_z \end{bmatrix}\cdot\begin{bmatrix} u_j\\ v_j\\ w_j\end{bmatrix}\\
&=\begin{bmatrix} \phi_A - \phi_B\\ \phi_A - \phi_C\\ \left.\dfrac{\partial\phi}{\partial n}\right|_{\text{node i}}\end{bmatrix},
\end{aligned} \tag{12}$$

where $\nabla\phi_j$ is replaced by $\boldsymbol{\nu}_j = (u_j, v_j, w_j)$, so the velocity vector of element j can be obtained by solving the equation. However, there are many elements around node i so that different velocity vectors will be obtained from the equations of every element. Thereby, the velocity that is the closest to the actual velocity needs finding out at node i. The actual velocity of node i can be obtained by averaging the velocities of the elements around node i with the inverse of the area element S_j surrounding node i being weights, and it can be expressed as

$$\nu_i = \frac{\sum\limits_{\substack{\text{elements}\\ \text{All surrounding}}}\begin{bmatrix} u_j\\ v_j\\ w_j\end{bmatrix}\frac{1}{S_j}}{\sum\limits_{\substack{\text{elements}\\ \text{All surrounding}}}\frac{1}{S_j}}. \tag{13}$$

The area element S_j can be obtained from the following formula:

$$S_j = \frac{1}{2}\left|(\boldsymbol{r}_A - \boldsymbol{r}_C)\times(\boldsymbol{r}_A - \boldsymbol{r}_C)\right| = \frac{J}{2}, \tag{14}$$

where J is the Jacobi's transformation of element j.

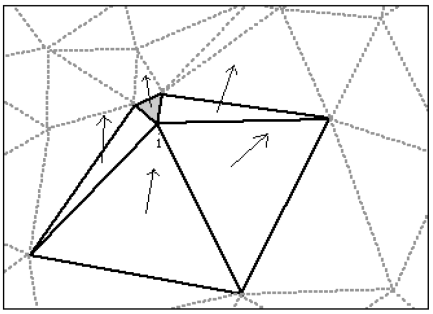


Fig.3. Node i, surrounded by 5 elements, with a very small element.

When choosing the weight coefficient, we choose $1/S_j$ instead of S_j, as shown in Fig.3. That is because there are 5 elements around node i and the area of the grey element is very small. Obviously, the element of smaller area has a greater influence on the normal vector of node i than the element of larger area, for the element of smaller area is closer to node i. If S_j is chosen as the weight number, the contribution of smaller element will be very little, and then the result would be distorted. So it is better to choose $1/S_j$ as a weight number. Normal vector of node i can be obtained by using a similar method as follows:

$$\boldsymbol{n}_i = \frac{\sum\limits_{\substack{\text{elements}\\ \text{All surrounding}}}\boldsymbol{n}_j\frac{1}{S_j}}{\sum\limits_{\substack{\text{elements}\\ \text{All surrounding}}}\frac{1}{S_j}}. \tag{15}$$

This method can assure the convergence of solution. With the linear average method,[17] the normal can be approximately obtained by averaging the normal vectors of the elements surrounding the node, but this method is not accurate. In a grid refinement

process, the solution will diverge. The accuracy depends on the regularity of its surrounding elements. After all, the 'true' normal of a polyhedron's vertex is uncertain. We calculate the velocity without using the nodal normal, so this difficulty is avoided. After the grids have been determined, the velocities of all elements approach the accurate values, and then the convergence of the solution to the equation can be guaranteed. After the velocity of boundary surface has been known, the next location of boundary surface can be obtained by the forward-advancing method in time domain.

4. Results and discussion

4.1. Analysis of the convergence of the size of the boundary

The size of the free surface will directly influence the accuracy of calculation with the BEM. Therefore, in this paper, the effect of free surface size on the accuracy of calculation is studied above all. The maximum radius of the bubble is assumed to be $R_{\rm m}$ and the size of the free surface is set to be multiples of the maximal radius of bubble, i.e. 2–15 times as large as the maximum radius of bubble. The convergence is analysed with the calculation result as shown in Fig.4.

From Fig.4 it can be seen that when the size of the free surface is larger than 6 times as large as the maximal radius of bubble, the calculation error can be controlled within 0.2%. Therefore, the size of the free surface is set to be 6 times as large as $R_{\rm m}$.

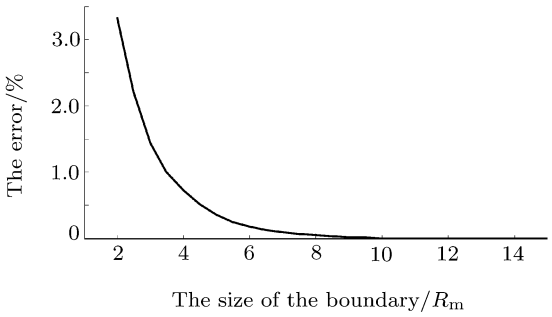
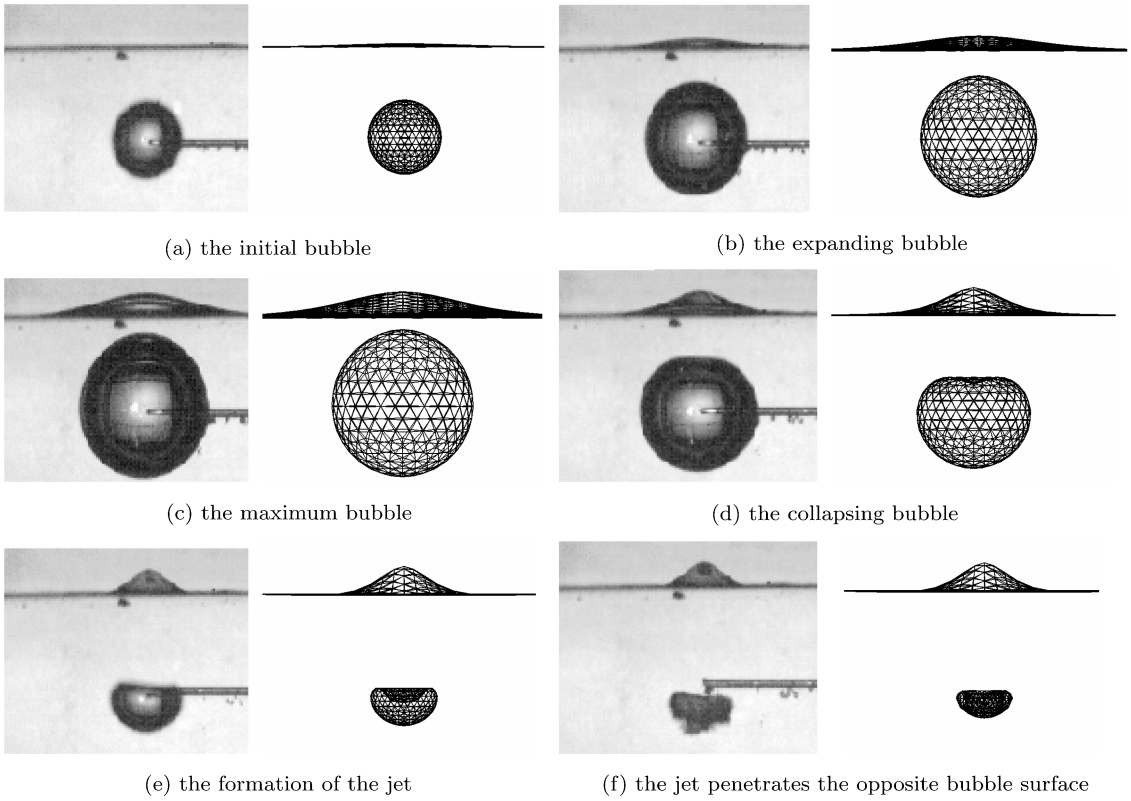


Fig.4. Analysis of the convergence of the boundary size.

4.2. Comparison between the calculation results and experimental results

There is little literature involved with the experimental research or the numerical research on the dynamics of high-pressure bubbles close to the free surface. In order to verify the numerical model in this paper, the calculation results from the numerical model in this paper are compared with the experimental results. The testing parameters will be transformed into dimensionless parameters which are $R_0 = 0.1651$, $\varepsilon = 100$, $\delta^2 = 0$, and $\gamma_f = 1.1$. In order to better compare the bubble shape obtained from the numerical simulation with that from the experiment, the numerical simulation should be carried out in synchronism with the experiment, and the detailed evolving process is shown in Figs.5(a)–5(f).

Figure 5(a) shows the initial state of the bubble and the free surface, when the temperature and the pressure inside the bubble are high and the bubble expands quickly outwards. Figure 5(b) shows the state of the expansion phase and the free surface, when the bubble continues to expand because of the inertia effect and interacts with the free surface. The free surface rises to form a spike, which is the phenomenon the same as that described in Cole's book.[18] But the bubble keeps nearly spherical, which illuminates that the free surface and the gravity have little influence on the expanding phase of the bubble. Figure 5(c) shows that the bubble reaches its maximum volume with the inner pressure being minimum. The upper bubble surface is attracted by the free surface. Figure 5(d) shows that the bubble begins to collapse and the free surface continues to rise. Figure 5(e) shows that the bubble is repelled by the free surface and a downward jet is formed. Figure 5(f) shows that the bubble collapses quickly and the jet penetrates through the other side of the bubble wall, turning into a toroidal bubble. In a word, in the expansion phase, the free surface has little influence and the bubble keeps nearly spherical, while in the collapse phase, the Bjerknes force of the free surface is more aggravated the bubble collapses and generates a jet and the jet penetrates into the opposite bubble surface.



(a) the initial bubble (b) the expanding bubble

(c) the maximum bubble (d) the collapsing bubble

(e) the formation of the jet (f) the jet penetrates the opposite bubble surface

Fig.5. The interaction between the bubble and the free surface.

4.3. Interaction of two in-phase bubbles

In the past decades, a vast literature about single bubble dynamics has been published. But, relatively, there has been little research on the interaction of double bubbles or multiple bubbles. The interaction between two bubbles exists in both the small bubbles and the macro large bubbles. For example, two charges exploding simultaneously can cause two in-phase bubbles. In order to study the dynamics of bubbles generated by two charges exploding, the cases of shadow water and deep water are studied in this section.

4.3.1. Without a free surface

In deep water, the free surface influence can be ignored when the distance between the bubble and the free surface is over two times as large as the maximal radius of the bubble. To study the interaction between two bubbles under the action of gravity, the non-dimensional parameters of these two bubbles are taken as $R_0 = 0.1195$, $\varepsilon = 183$, $\delta^2 = 0.184$. The distance between the bubble centres is set to be 1.8. The bubble surface is discretized into 1280 three-node plane triangle elements and the time step is set to be 0.02. The calculation results are given in the non-dimensional form and the interaction between two in-phase bubbles is shown in Fig.6.

Figure 6(a) shows the initial state of the two bubbles at $t = 0$ and the contour shows the amplitude of the velocity potential of the bubble boundary. Figure 6(b) shows the state of bubbles at $t = 0.39$. In the expansion process, bubbles each take on a flat shape on their two opposite sides, keeping nearly spherical. Figure 6(c) shows the state at $t = 1.09$ when the bubble volumes reach a maximum and the interaction occurs between the two bubbles. They repel each other in the expansion phase, and then the bubbles are no longer spherical. Figure 6(d) shows the state at $t = 2.01$ when the bubbles begin to collapse and dent inwards, and then jets are formed. Figure 6(e) shows the state at $t = 2.22$ when the bubble collapse and jets are formed. The directions of jets are oblique, and the jets repel each other because of the influence of the gravity and the interaction between the bubbles. Numerical smoothing is not needed in the whole simulation process, which indicates that the BEM has a good adaptability when combined with the Elastic

Mesh Technique (EMT).[8] Figure 6 shows the whole process of expansion and collapse of these two bubbles under the action of gravity.

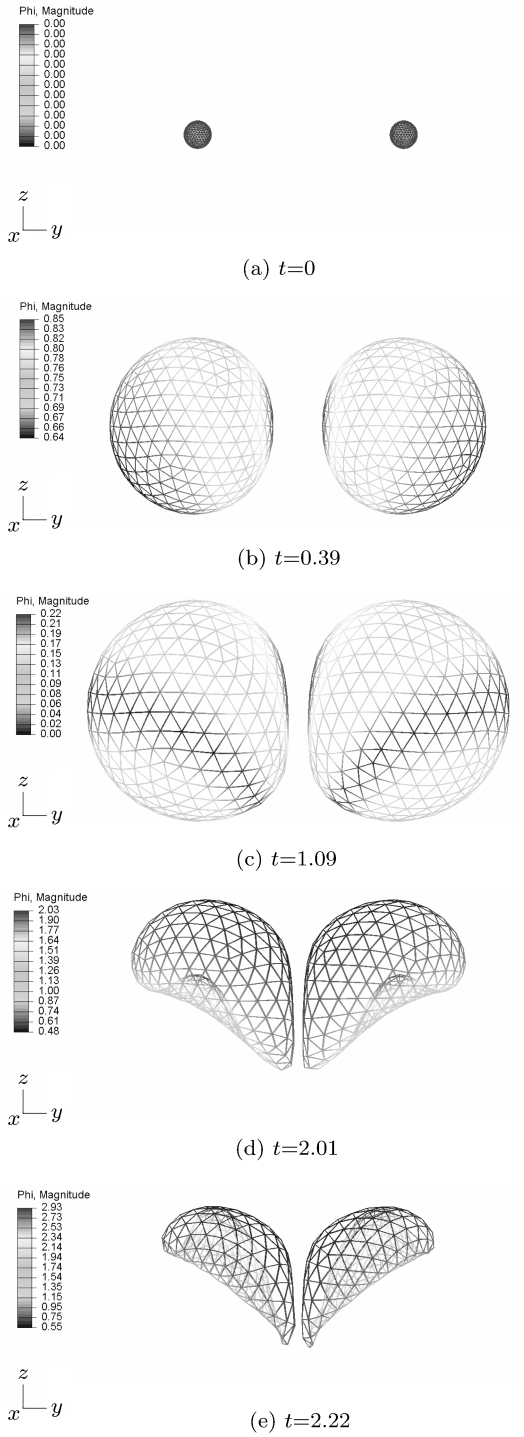


Fig.6. The interaction between two in-phase bubbles.

To study the effect of the distance between two bubbles on the bubble dynamics, the bubble non-dimensional period and the variation tendency of bubble centres along the z direction are computed with different values of distance d. The results are shown in Figs.7 and 8.

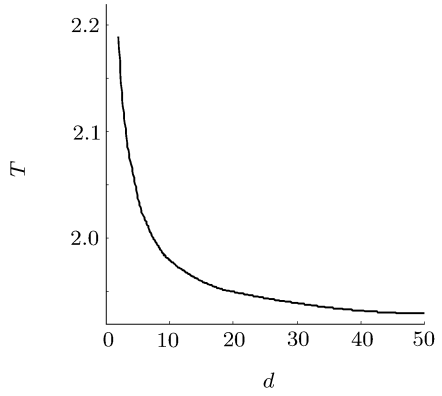


Fig.7. The variation of bubble period with distance between two bubbles.

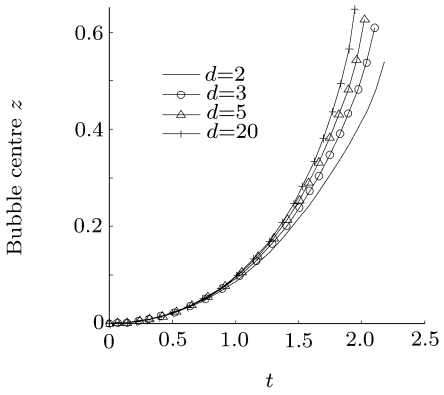


Fig.8. The vertical displacement variation of bubble centre with distance between two bubbles.

From Fig.7 it can be seen that the pulsation period increases with the decrease of the distance between the two bubbles. This is because that these two bubbles repel each other in the expansion phase but attract each other in the collapse phase, which restrains the motion of the bubble. From Fig.8 it can be seen that the displacements of bubble centres in the vertical direction decrease with the increase of the distance between the two bubbles. Therefore, the repulsion and the attraction restrain the motion of the bubbles, increasing the period of the bubble motion.

4.3.2. With a free surface

The motion of the underwater bubble is very complicated, especially when the bubble is close to a free surface, because the bubble will interact strongly with the free surface. For instance, when a charge explodes near the free surface, a water spike of metres will

be generated, but this special physical phenomenon is hard to observe and measure through experiment, especially for the case of multiple bubbles. Therefore, this specific underwater phenomenon is simulated with a three-dimensional model developed here. On the basis of last subsection, taking the effect of the free surface into account, we set the non-dimensional distance between the bubble and the free surface to be 1.0 and discretize the bubble surface into 1280 three-node plane triangle elements. The non-dimensional length and width of the free surface are both set to be 6 and the free surface is discretized into 690 three-node plane triangle elements. The calculation results are given in the dimensionless form. The interaction processes of bubbles and the free surface are shown in Fig.9.

Figure 9(a) shows the initial states of bubbles and the free surface at $t = 0$ where t is the non-dimensional time. The contour shows the non-dimensional amplitudes of velocity potential of the bubble boundary and the free surface. Figure 9(b) shows the states at $t = 0.28$ when the bubbles keep expanding and couple with the free surface. The free surface rises and the two bubbles repel each other, keeping spherical. Figure 9(c) shows the states at $t = 0.8$ when the bubble volumes each reach a maximum and couple with each other. Bubbles are attracted by the free surface and the bubbles are no longer spherical because of the repelling force between the two bubbles. Figure 9(d) shows the states at $t = 1.32$ when bubbles begin to collapse and the free surface rises more. The upper surfaces of the bubbles form downward jets under the joint action of the Bjerknes force and the gravity while the bottom surfaces each take on a flat shape because the Bjerknes force acts more strongly than the gravity. Figure 9(e) shows the states at $t = 1.57$ when bubbles collapse and jets are formed. The directions of jets are different from those described in the last subsection. In the last subsection, there is only gravity so the jet directions are reversed to the direction of gravity but here the jets are obliquely downward. Moreover, the bubble period is shortened obviously because of the joint action of the free surface and the gravity. Meanwhile, the free surface reaches the highest and the maximal non-dimensional displacement of the vortex of the free surface is 0.67 which is 0.67 times as large as the maximum radius of bubble, about 4m.

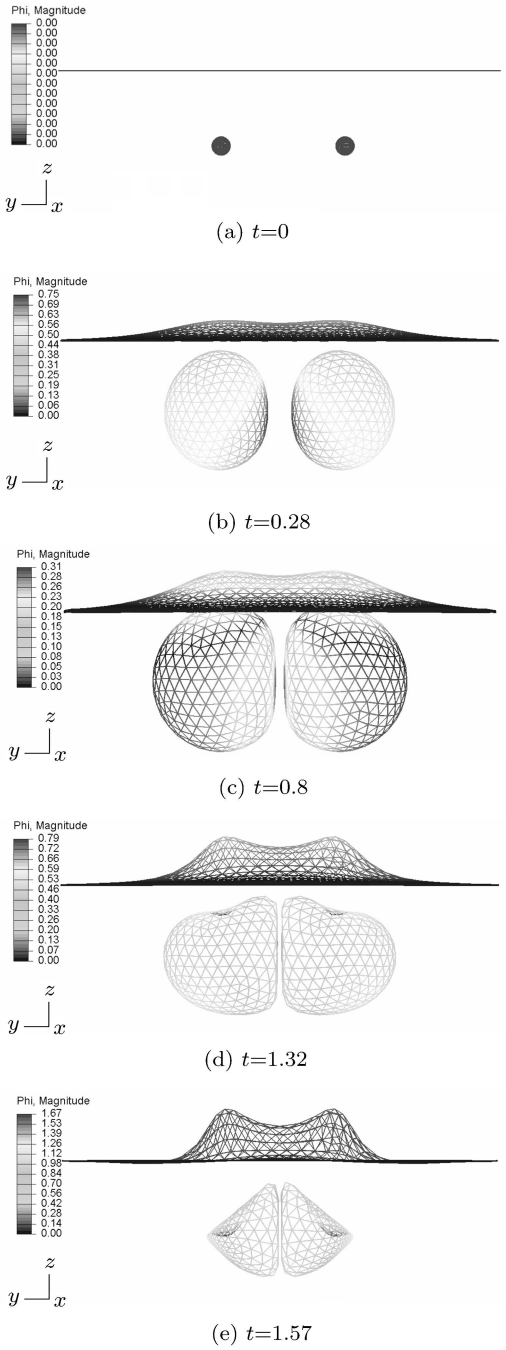


Fig.9. The interaction between two in-phase bubbles near free surface.

4.4. Interaction between two out-phase bubbles

Here the two out-of-phase bubbles are generated by two charges exploding in water continuously. To study the dynamics of the two bubbles, this section will be dedicated to the explosion cases in shadow water and deep water separately.

4.4.1. Without a free surface

Ignoring the free surface effect, we mainly study the interaction between two out-of-phase bubbles underwater explosion. Non-dimensional parameters of bubbles are $R_0 = 0.1195$, $\varepsilon = 183$, and $\delta^2 = 0.184$. And the non-dimensional distance between the bubbles is 1.8. The bubble surface is discretized into 1280 three-node plane triangle elements. Time step is set to be 0.02 and the non-dimensional time between two explosions is 0.007. Calculation result is given in the dimensionless form. The interaction process of the two out-of-phase bubbles is shown in Fig.10.

Figure 10(a) shows the states of the two bubbles at $t = 0.02$, and the contour shows the amplitude of the velocity potential at the boundary, from which we can see that one of bubbles explodes first. Figure 10(b) shows the states at $t = 0.40$. Bubbles expand further, and the right bubble takes on a flat shape on each of two sides, but the left one keeps nearly spherical. Figure 10(c) shows the states at $t = 0.96$ when the bubble volumes each reach a maximum, and the interaction occurs between the two bubbles. They repel each other in the expanding phase, depressing the motion of the right bubble (which explodes later). The bubbles are no longer spherical. Figure 10(d) shows the states at $t = 1.25$ when the bubbles begin to collapse and the right bubble dents inwards, and then a jet is formed, but the left bubble keeps nearly spherical. Figure 10(e) shows the states at $t = 1.37$ when the right bubble collapses and a jet is formed. The jet is oblique under the gravity and the interaction between bubbles. In this case, the right bubble is created 0.007 later than the left bubble, and this is the only difference between this out-of-phase case and that in-phase case in the last subsection. However, there is a great difference in interaction between the two different cases. For example, the period of the bubble generated early increases and that of the bubble generated later decreases greatly. The motion of the bubble generated later is restrained by the bigger bubble, making it collapse too early and then weakening its power. In this paper it is called the depression effect between two out-of-phase bubbles, which can give a reference to the research on the power generated by multiple charges exploding simultaneously or continuously.

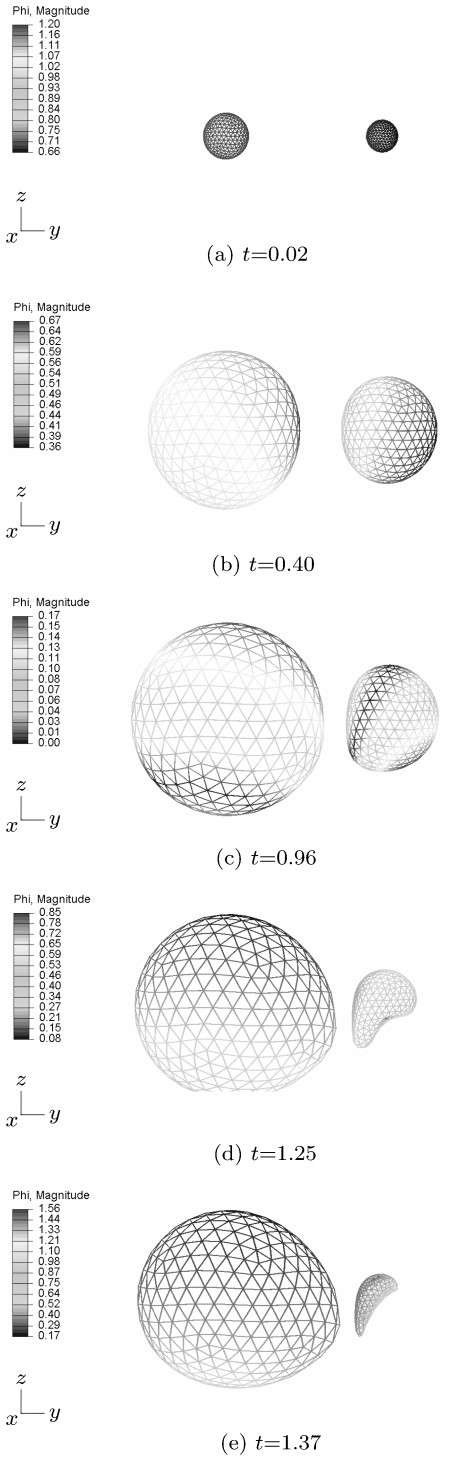


Fig.10. The interaction between two out-of-phase bubbles.

4.4.2. With a free surface

To better simulate the bubble dynamics, we take the effect of free surface into account and set the non-dimensional distance between the bubble centre and the free surface to be 1, and we discretize the bubble surface into 1280 three-node plane triangle elements. The non-dimensional length and width of the free surface are both set to be 6, and the free surface is discretized into 690 three-node plane triangle elements. The calculation results are given in dimensionless form. The interactions between the two out-of-phase bubbles near the free surface are shown in Fig.11.

Figure 11(a) shows the states of bubbles and the free surface at $t = 0.02$ where t is the non-dimensional time. The contour shows the non-dimensional amplitudes of the velocity potential of the bubble boundary and the free surface. Figure 11(b) shows the states at $t = 0.40$ when the bubbles continue expanding and couple with the free surface. The free surface rises and the two bubbles repel each other. The right bubble is nearly spherical and the left one takes on a flat shape. Figure 11(c) shows the states at $t = 0.72$ when the left bubble volume reaches a maximum and couples with the free surface. Bubbles are attracted by the free surface, and the bubbles repel each other, which restrains the motion of the right bubble which is generated later. Figure 11(d) shows the states at $t = 0.90$ when free surface rises more. The left bubble is still nearly spherical while the right bubble begins to collapse under the joint action of the Bjerknes force and gravity. The upper surface and the bottom surface each take on a flat shape. Figure 11 (e) shows the states at $t = 1.01$ when the right bubble collapses under the action of the left bubble. Owing to the fact that the water volume of the free surface is excluded by the bubbles, the retarded flow is weakened and the energy supplied by the retarded flow is reduced, which results from the depression effect of the left bubble on the right bubble. In last subsection, there exists only the gravity so that jets reversed to the gravity are generated. But in this subsection, the Bjerknes force is counteracted with the gravity so that no jet is formed. Moreover, the periods of bubbles are shortened obviously because of the joint action of the free surface and the gravity of bubbles.

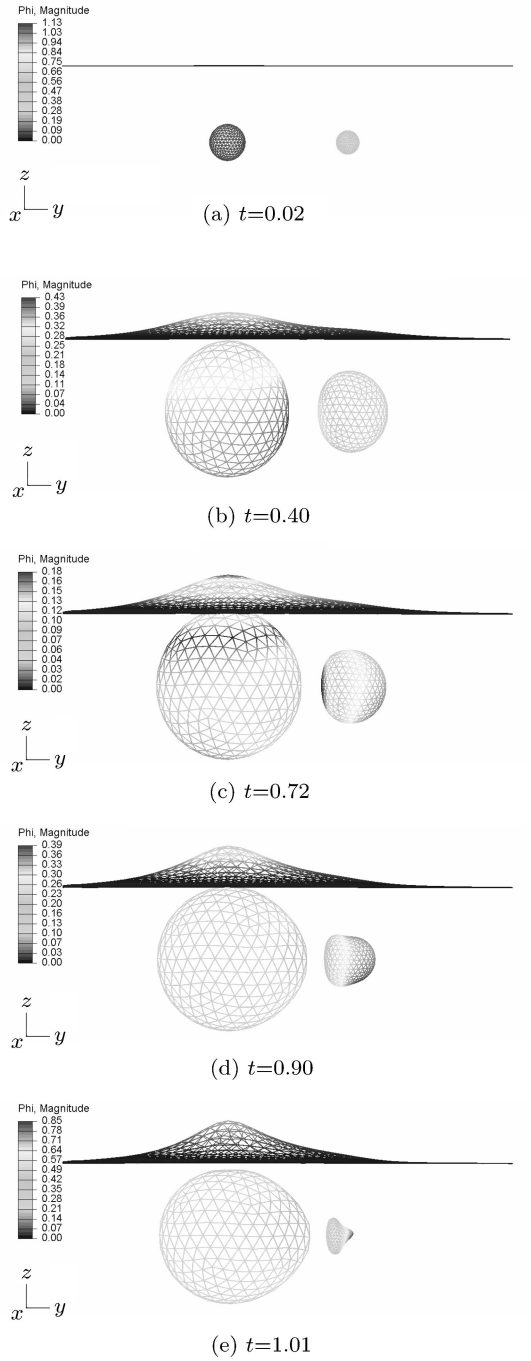
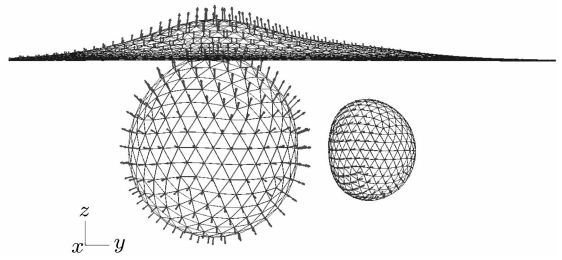
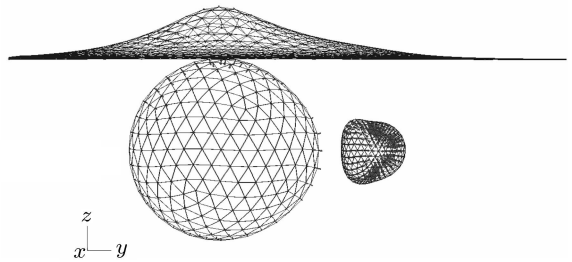


Fig.11. The interaction between two out-of-phase bubbles near free surface.

To better observe the interaction between the two bubbles and the free surface, the velocity vectors at the boundary at $t = 0.56$ and 0.90 are shown in Fig.12.



(a) t=0.56



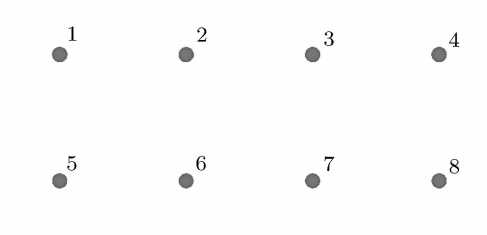
(b) t=0.90

Fig.12. The velocity vectors of two out-of-phase bubbles near surface.

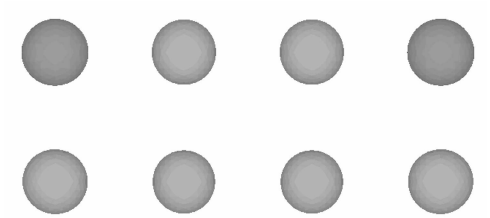
From the velocity vectors it can be seen that the right bubble begins to collapse at $t = 0.56$ while the left bubble continues expanding and the free surface rises. Bubbles enter collapse phase at $t = 0.90$; the right bubble collapses too early which leads the power to be weakened. In addition, the right bubble makes no contribution to the water-grave phenomenon. This is because of the depression effect from the interaction between these two out-of-phase bubbles. Therefore, it can be concluded that the depression effect exists between two out-of-phase bubbles, whether there exists a free surface or not.

5. Interactions of multiple bubbles

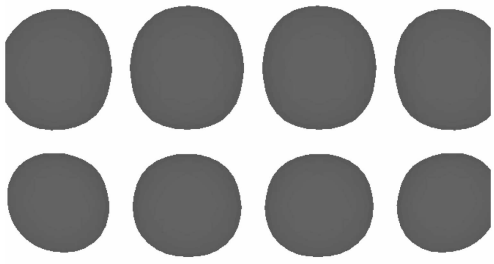
For the next example, we aim to simulate the bubble dynamics large-scale problem by using the present numerical method. The dimensionless parameters of eight bubbles are $R_0 = 0.1195$, $\varepsilon = 200$, and $\delta^2 = 0.25$. The dimensionless distance between two bubble centres is 2 and the bubble surface is discretized into 1280 three-node plane triangle elements and the time step is 0.02. The calculation results are given in the dimensionless form as shown in Fig.13.



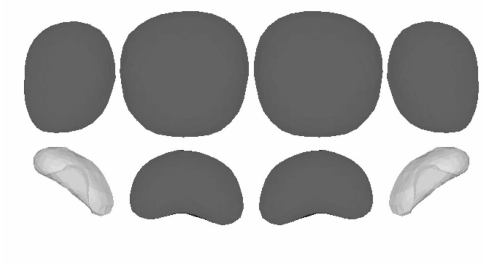
(a) t=0



(b) t=0.3



(c) t=1.1



(d) t=1.7

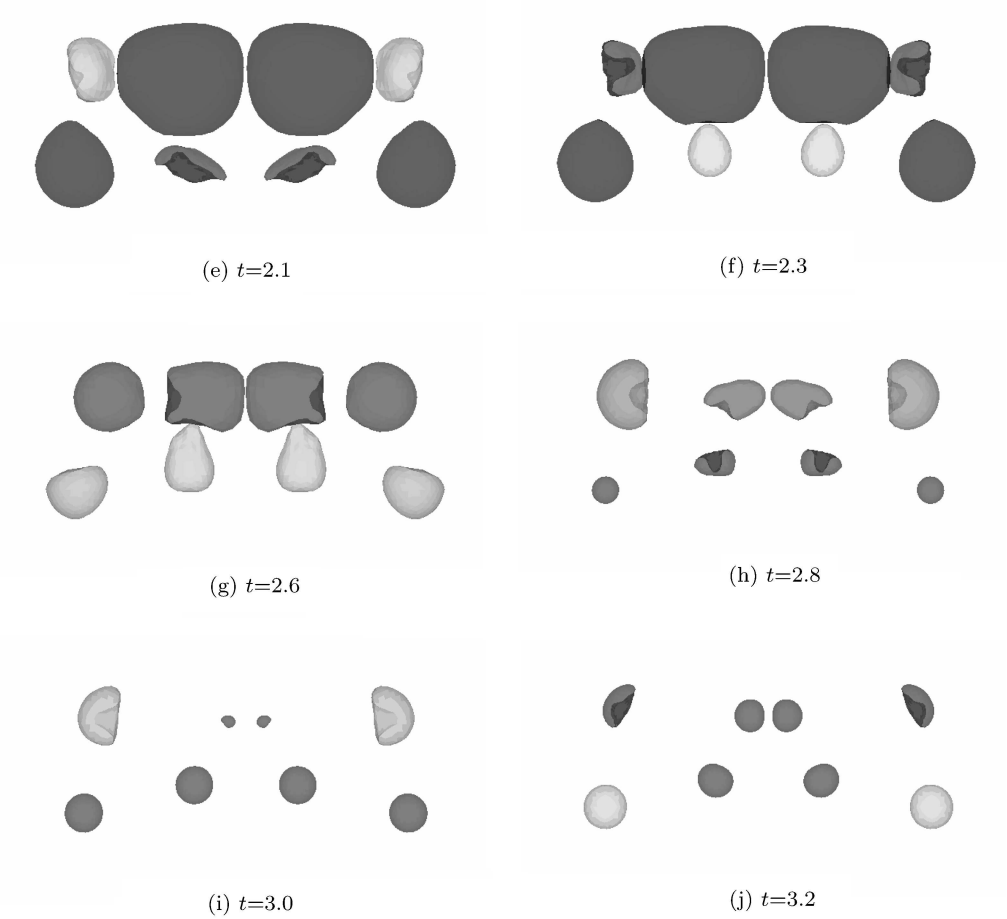


Fig.13. The interaction among multiple bubbles.

Figure 13 shows the strong coupling effects of multiple bubbles including expansion, collapse, jet formation and rebound process. The periods of motion and the directions of jets are different because of the interaction of bubbles. For example, the motion periods of bubbles 2 and 3 are longest and those of bubbles 6 and 7 are shortest, and also the bubble shapes are different. This work just does some original research on the interaction among multiple bubbles, and further research about the complex physical phenomenon of multiple bubble interaction will be done in the future work.

6. Conclusions

Based on the potential flow theory, the dynamics of the bubbles is simulated with the BEM, and a 3D code is developed. Calculation results agree well with the experimental results. With the present numerical method, the interactions of multiple bubbles are simulated, including in-phase bubbles and out-of-phase bubbles. Main suggestions and conclusions are as follows:

1) The numerical error is less than 0.2% when the size of the free surface is set to be larger than 6 times as large as the bubble maximal radius.

2) The periods of the bubble motion increases with the decrease of the distance between the two bubble centres.

3) The vertical displacement of the bubble centres also decreases with the increase of the distance between the two bubble centres.

4) Underwater bubble interacts with the free surface strongly when close to it, and the free surface forms a water spike under the action of an underwater bubble, and forms double peaks under the action of two bubbles.

5) Under the joint action of the Bjerknes force and the gravity, there appears the depression effect in multiple bubbles, especially for out-of-phase bubbles, whether there exists a free surface or not.

6) The interaction between two out-of-phase bub-

bles is quite different from that between two in-phase bubbles because of the depression effect. For the bubbles generated in underwater explosion, the period of the bubble formed first increases while that of the bubble formed later decreases greatly. The larger bubble restrains the motion of another bubble, which makes the bubble formed later collapse too early and weaken its power.

7) Jets in different directions are formed under the strong interaction among multiple bubbles. These physical phenomena give a reference to the research of the power of multiple weapons exploding simultaneously or continuously.

References

[1] Zhang Y L, Yeo K S, Khoo B C and Chong W K 1998 *Comput. Phys.* **146** 105

[2] Klaseboer E, Hung K C, Wang C, Khoo B C, Boyce P and Debono S 2005 *J. Comput. Phys.* **194** 451

[3] Wang C and Khoo B C 2004 *J. Comput. Phys.* **194** 451

[4] Lu C J 1996 *Chin. J. Aeron.* **9** 38 (in Chinese)

[5] Xiao Z Y and Reginald B H 2005 *Chem. Eng. Sc.* **60** 179

[6] Best J P and Kucera G C 1992 *J. Fluid Mech.* **245** 137

[7] Wu X M, Ying C F and Li C 2005 *Chin. Phys.* **14** 5

[8] Wang C, Khoo B C and Yeo K S 2003 *Computers and Fluids* **32** 1195

[9] Wang Q X, Yeo K S, Khoo B C and Lam K Y 1996 *Theor. Comput. Fluid Dynam.* **8** 73

[10] Wang Q X, Yeo K S, Khoo B C and Lam K Y 1996 *Comput. Fluid* **25** 607

[11] Gao B, Zhang H H and Zhang C 2003 *Acta Phys. Sin.* **52** 14(in Chinese)

[12] Liu H J and An Y 2004 *Acta Phys. Sin.* **53** 5(in Chinese)

[13] Rungsiyaphornrat S, Klaseboer E, Khoo B C and Yeo K S 2003 *Comput. and Fluids* **32** 104

[14] Yao X L and Zhang A M 2006 *J. Theor. Appl. Mech.* **38** 749 (in Chinese)

[15] Yao X L and Zhang A M 2006 *J. Mar. Sci. Appl.* **5** 14

[16] Zhang Y L, Yeo K S, Khoo B C and Wang C 2001 *J. Comput. Phys.* **166** 336

[17] Harris P J 1992 *J. Num. Methods Eng.* **33** 1813

[18] Cole R H 1948 *Underwater Explosion* (Princeton, NJ: Princeton University Press) p80